Ionization, excitation of high-lying atomic states, and molecular fluorescence in Cs vapor excited at $\lambda=455.7$ and 459.4 nm

J. Huennekens,* Z. Wu, and T. G. Walker
Department of Physics, Princeton University, Princeton, New Jersey 08544
(Received 16 July 1984)

We have studied in detail the ionization and population of high-lying atomic states which occur in cesium vapor excited at the second resonance transition, $6S$-$7P$. We have developed a simple model which qualitatively explains the laser-power dependences of level populations and electron densities which we observed. Measurements of spatial dependences of fluorescence point out the critical role of radiation trapping in these phenomena. Similar observations on rubidium demonstrate the same type of behavior when the first ($5S$-$5P$) or second ($5S$-$6P$) resonance is excited. At higher densities and temperatures we found that the fluorescence was dominated by diffuse molecular bands. Some of these bands probably consist of transitions to the repulsive $^3\Sigma_u^+$ state. Additionally four bands observed at 817.5, 826.6, 835.3, and 839.6 nm are tentatively identified as the cesium analog of the $^3\Pi_g \rightarrow {}^3\Sigma_u^+$ satellite bands which have previously been observed in the blue wing of the first resonance doublet of the lighter alkali metals.

I. INTRODUCTION

Resonant laser excitation is a very efficient technique for coupling energy into a vapor. In 1976 Allegrini *et al.*[1] observed fluorescence from high-lying atomic levels in sodium vapor excited with a cw laser tuned to the first resonance transition. The population of these high-lying levels was attributed to excited-atom—excited-atom "energy pooling" collisions of the form $\mathrm{Na}(3P)+\mathrm{Na}(3P) \rightarrow \mathrm{Na}(3S)+\mathrm{Na}(nL)$. At about the same time, Lucatorto and McIlrath[2] observed a very efficient and almost complete ionization of Na vapor excited to the first resonance level by a high-power, pulsed laser. Measures[3] suggested that the mechanism of this ionization is electron-impact ionization of excited atoms by fast electrons which have previously been heated by one or more superelastic collisions: $\mathrm{Na}(3P)+e^-(E) \rightarrow \mathrm{Na}(3S)+e^-(E+2.1\ \mathrm{eV})$. More recently it has been shown that associative[4–8] and Penning[9–11] ionization, photoionization,[12] and other ionization mechanisms can be important in resonantly excited vapors. In optically thick vapors excitation transfer from atoms to molecules[13] can be important due to the high density of diatomic molecules (a few tenths to a few percent of the atomic number density) and the long effective (trapped) radiative lifetimes of the atomic states. Additionally stimulated processes can become important when a population inversion is created directly by the laser pumping[14–16] or by selective collisional processes.[17,18]

We report here the systematic study of cesium vapor excited at the second resonance transition $6S_{1/2} \rightarrow 7P_{3/2}$ ($\lambda=455.7$ nm) or $6S_{1/2} \rightarrow 7P_{1/2}$ ($\lambda=459.4$ nm) by a cw dye laser. Most of the above-mentioned processes are observed with different ones becoming dominant as the temperature, cesium number density, laser power, laser detuning, and foreign-gas pressure are varied.

At relatively low cesium number densities, $6\times10^{13} < n < 4\times10^{15}$ cm^{-3}, Sharma *et al.*[14] observed "mirrorless lasing" on the $7P \rightarrow 7S$, $7P \rightarrow 5D$, and $7S \rightarrow 6P$ transitions (see Fig. 1) where the population inversion was directly produced by the cw laser pumping at $\lambda=455.7$ or 459.4 nm. They observed that the lasing rapidly turned off as either foreign gas was introduced, or the cesium number density exceeded 4×10^{15} cm^{-3}. This turnoff is due to collisional mixing of the upper and lower laser levels although in the case of increasing Cs density this is compounded by increasing radiation trapping which slows the decay of the lower levels.

In the temperature range 235—335 °C, corresponding to cesium densities 6×10^{15}—8×10^{16} cm^{-3}, radiation trapping becomes more severe and collision rates exceed effective radiative rates. In this temperature region a striking phenomenon occurs which has been observed previously in this laboratory[20,21] and possibly in others,[22] but has never been adequately explained. For the first centimeter or so of the vapor cell, the usual blue resonance radiation seen at lower temperatures is completely overshadowed by a much more intense red ball of fluorescence. This "red glow" extends far outside the laser-excited column and is due to fluorescence from a large number of highly excited states. Additionally, the blue, free-bound recombination continuum $\mathrm{Cs}^+ + e^- \rightarrow \mathrm{Cs}(6P) + h\nu$ is observed, indicating that electrons are present in significant numbers. This phenomenon is related to the "quasiresonant" ionization reported by Tam and Happer[23,24] and the two-photon ionization observed by Bahns and Stwalley[25] and Koch *et al.*[26] as well as the pulsed Lucatorto and McIlrath experiment.[2] However, it appears in the present case that rather than creating a localized plasma spark at the focus of a laser beam, radiation trapping causes the ionization to spread well outside the laser beam and fill much of the cell. We have studied the laser power, temperature, and spatial dependences of the high-level fluorescence and of the electron density. We have also qualitatively studied the effects of foreign gas on these phenomena. These re-

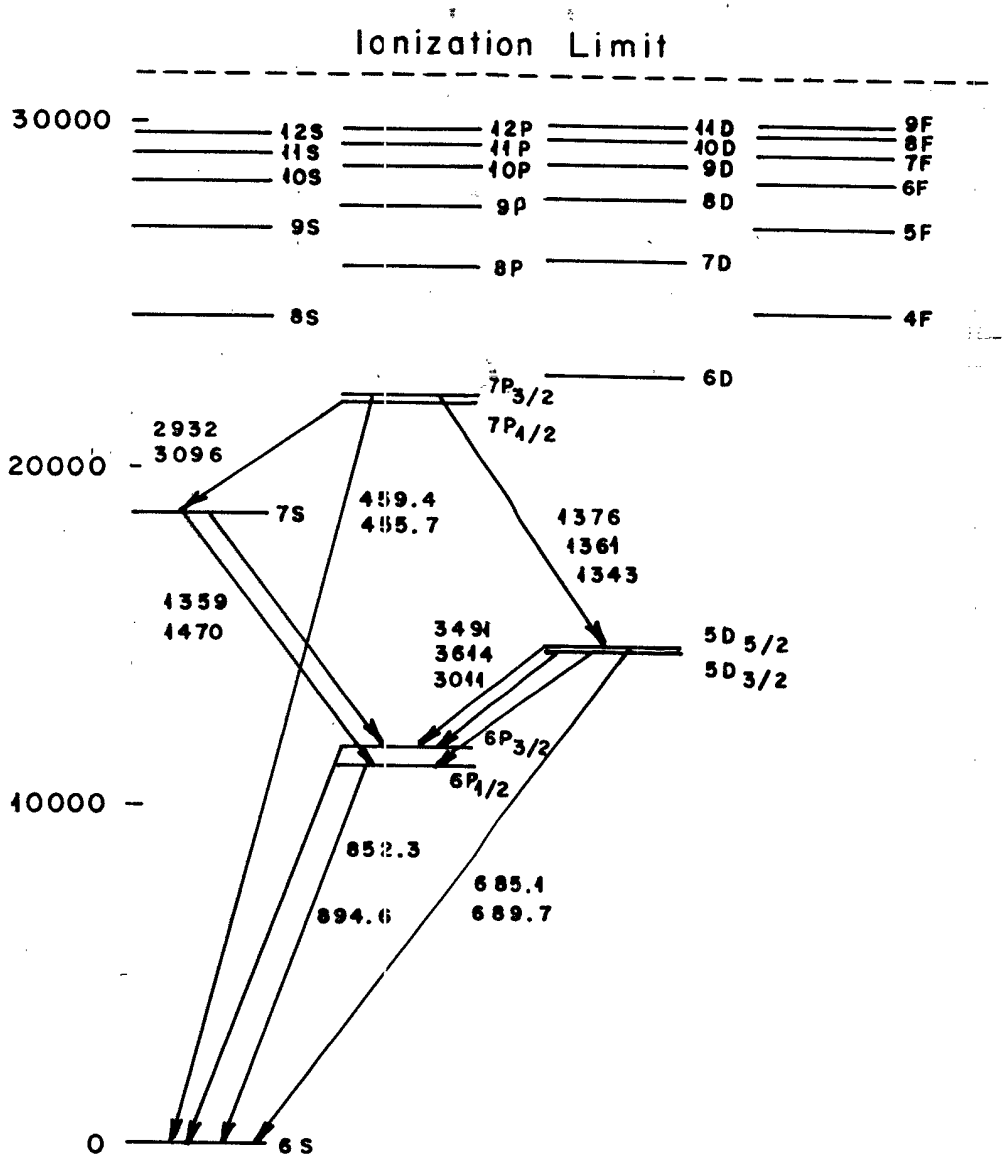

FIG. 1. Cesium energy-level diagram with energies (in cm^{-1}) taken from Ref. 19. Transition wavelengths are in nm.

sults are presented in Sec. III. Additionally, we have developed a simple three-level model, described in Sec. IV, which incorporates electron-impact excitation, deexcitation and ionization, spontaneous decay and radiation trapping, excited-atom—excited-atom collisions, associative and Penning ionization, radiative recombination, and electron and ion diffusion. This model qualitatively reproduces our results.

At still higher cesium number densities, $n > 10^{17}$ cm^{-3}, radiation trapping of atomic fluorescence is so severe, and the Cs_2 number density so high, that the dominant decay mode of excited atoms is collisional excitation transfer to molecules. Densities in atomic levels are greatly reduced compared to the situation described in the preceding paragraph due to this rapid decay mechanism. Consequently ionization and electron-impact excitation are insignificant and the fluorescence spectrum consists almost entirely of Cs_2 bands. In this situation we have observed the well-known Cs_2 A, B, and E bands which have been studied extensively in absorption[27–32] and in fluorescence.[33] However, due to trapping of allowed molecular fluorescence to the ground state $X\,^1\Sigma_g^+$, these bands are somewhat suppressed. Conversely, the three narrow bands lying between 700 and 720 nm, which were attributed by Gupta *et al.*[32] to triplet-triplet transitions whose upper levels dissociate at large internuclear separation to $5D+6S$, are strong in the present spectra. A set of satellite bands between 810 and 840 nm, first reported in Ref. 27, is also strong, as is a double-peaked structure between 540 and 560 nm. Additionally we observe the main peak of the interference continuum at 610 nm which has been discussed in detail in Refs. 34—38. These data are presented in Sec. V.

II. EXPERIMENT

Figure 2 is a block diagram of the experimental apparatus. The cells are cylinders 2.5 cm in diameter, either 5 or 20 cm long and are made of Corning 1720 glass. The cells were baked for $\sim$12 h at greater than 580°C on a

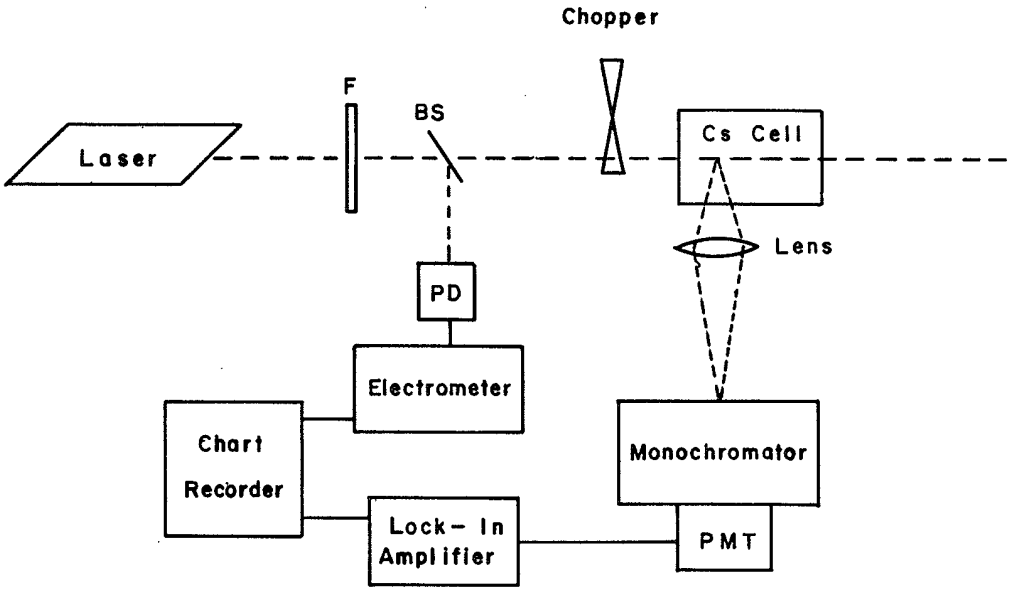

FIG. 2. Experimental setup. PMT, photomultiplier; PD, photodiode; F, neutral-density filter; BS, beam splitter.

vacuum system maintaining a pressure less than 10^{-6} Torr. A small amount of 99.9%-pure cesium metal was distilled into the cells before sealing. In most cases no buffer gas was added to the cells. We heated the cell with nichrome wire heaters in a Pyrex oven and monitored its temperature with a thermocouple attached to the cell tip with thermally insulating ceramic cement to prevent radiation heating of the thermocouple.

Either line of the second resonance doublet ($6S \rightarrow 7P$, $\lambda = 455.7$ or 459.4 nm) was excited using the multimode output of a stilbene 3 cw dye laser (Coherent 599-03) pumped by the uv lines of an argon-ion laser (Spectra-Physics model 171-19). The dye-laser output was ~ 200 mW with an ~ 20-GHz bandwidth. In Sec. IV we will briefly discuss similar experiments in rubidium vapor in which either the second resonance doublet ($5S \rightarrow 6P$, $\lambda = 420.3$ or 421.7 nm) was pumped with the stilbene dye laser or the first resonance doublet ($5S \rightarrow 5P$, $\lambda = 780.2$ or 795.0 nm) was pumped with a multimode oxazine cs dye laser (Spectra-Physics model 375) pumped by a Kr^+ laser (Spectra-Physics model 171-01). In the latter case, output power was ~ 300 mW and the laser bandwidth, ~ 30 GHz.

Fluorescence was observed at right angles to the laser beam with a 0.3-m scanning monochromator (McPherson model 218) and a cooled photomultiplier with an S-20 cathode response (EMI 9558). In most cases the laser beam was mechanically chopped and the photomultiplier anode current was amplified by a lock-in detector (PAR model 128) and displayed on a chart recorder. Alternatively, the photomultiplier current could be measured directly with a Keithley electrometer. An intrinsic germanium detector (North Coast model EO-917L) was used to obtain spectral information in the near infrared (0.8–1.6 μm). In the latter stages of the experiment a 0.85-m double monochromator (Spex model 1404) was used for increased resolution. The laser power was varied using calibrated neutral-density filters inserted at position F in Fig. 2 and constantly monitored after the filter by a photodiode (PD in Fig. 2).

III. EXPERIMENTAL RESULTS FOR THE IONIZATION AND POPULATION OF HIGH-LYING ATOMIC LEVELS

Figure 3 shows the full cesium emission spectrum from $\lambda = 360$ nm to $\lambda = 1.6$ μm produced when the vapor at $T \sim 247$ °C was excited at the $6S_{1/2} \rightarrow 7P_{3/2}$ resonance frequency. The spectrum is dominated by known atomic transitions from levels all the way up to the ionization limit. The bright red color of this fluorescence is due to the concentration of intense lines between $\lambda = 580$ and 730 nm. This red fluorescence is much brighter than the blue $7P \rightarrow 6S$ resonance fluorescence which dominates the spectrum if the laser is slightly detuned. Evidence of ionization is present in Fig. 3 in the plasma broadening of higher F levels and in the blue $Cs^+ + e^- \rightarrow Cs(6P) + h\nu$ recombination continuum[39] between $\lambda = 430$ and 510 nm. Also observed in the spectrum are a large number of "forbidden" transitions. The strongest of these is the $5D_{5/2,3/2} \rightarrow 6S_{1/2}$ doublet at 685.1 and 689.7 nm which was observed in emission by McClintock and Balling[40] 15 years ago following excitation of molecular transitions by various Ar^+ laser lines. However, we also observe the $6D_{5/2,3/2} \rightarrow 6S_{1/2}$ doublet at 442.7 and 441.9 nm and a series of weak doublets located on the short-wavelength side of the $nF \rightarrow 5D_{5/2,3/2}$ series which may be identified as the forbidden transitions $nG \rightarrow 5D_{5/2,3/2}$ with $n = 5$, 6, 7, and 8. For higher n, the F and G lines merge. In the case of $n = 6$ and 7, the G lines are split with the short-wave component being identifiable as the forbidden $nH \rightarrow 5D_{5/2,3/2}$ lines. The $6G \rightarrow 5D$ and $6H \rightarrow 5D$ lines may be seen in Fig. 8(b). Presumably these G and H states possess some F character due to Stark mixing of the wave functions, which allow this radiation to be observ-

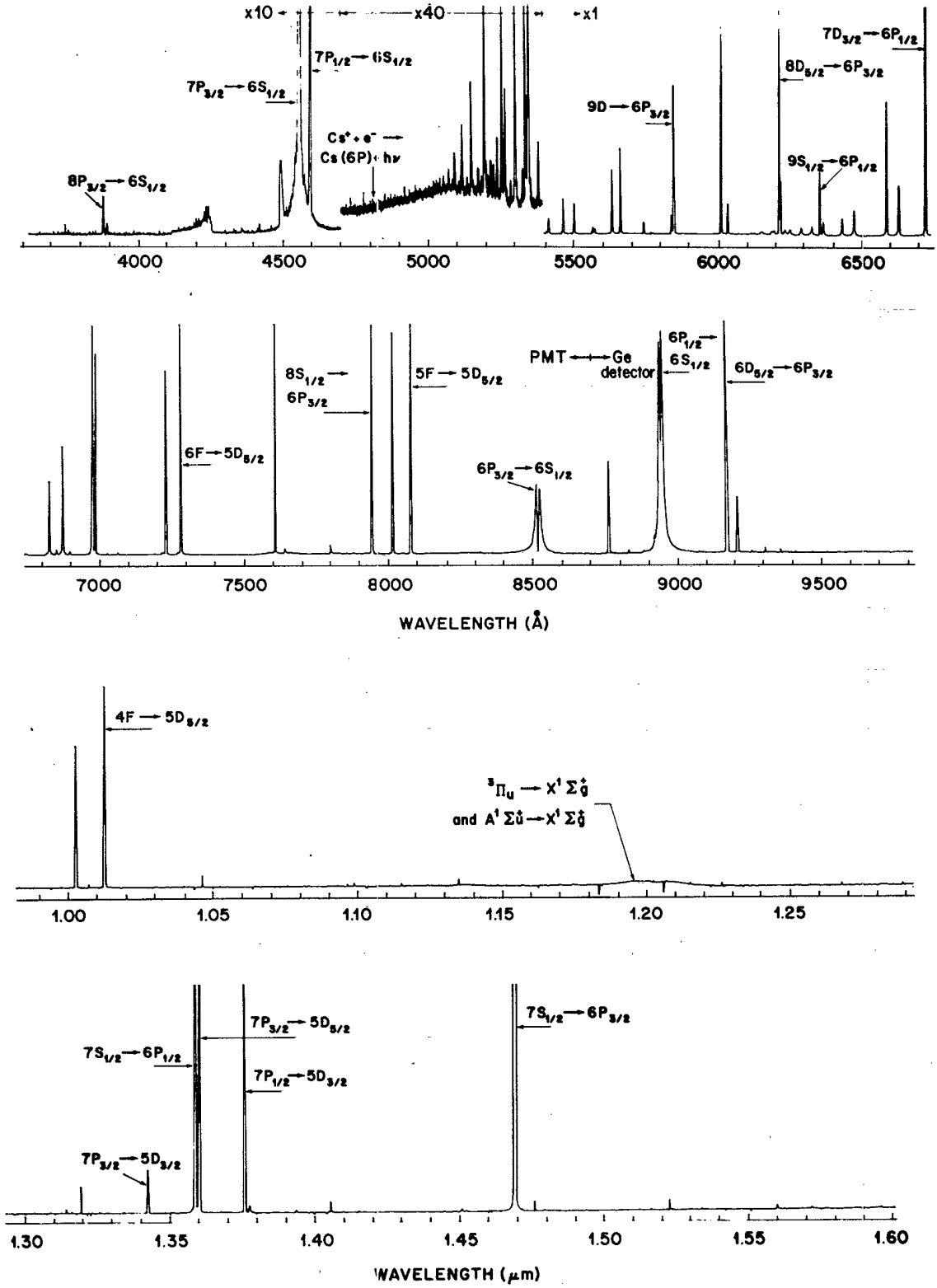

FIG. 3. Cesium emission spectrum from $\lambda=360$ nm to 1.6 μm, for laser excitation at $\lambda=455.7$ nm ($6S_{1/2} \rightarrow 7P_{3/2}$). $T=247$°C. The broad feature near 420 nm is an artifact of the monochromator grating.

able. The proximity of F and G states at higher n is also responsible for the large Stark broadening of higher F lines discussed below. Finally, we also observe the very weak forbidden transitions $nP_{3/2} \rightarrow 6P_{3/2}$ for $n=9$, 10, and 11.

From the spectra such as shown in Fig. 3, we measured relative intensities of the various atomic lines, corrected for the detection-system efficiency. Since intensities were obtained from peak heights (with the exception of $6P \rightarrow 6S$ where areas were measured), we expect some un-

derestimation of intensities of transitions from higher F levels which are Stark broadened beyond the resolution of the monochromator. To obtain relative populations (plotted in Fig. 4) we used transition probabilities taken from Warner[41] and Fabry.[42] For transitions to the ground state, radiation trapping effects are important and values of those effective radiative rates were estimated using Holstein's theory of radiation trapping.[43,44] Trapping in transitions to the $6P$, $7S$, and $5D$ states is also nonnegligible but is very difficult to estimate due to the far from ideal spatial distributions of atoms in those states. (Holstein's theory considers radiation trapping by a uniform distribution of atoms in an infinite slab or infinite cylinder geometry. In our case the geometry is not infinite and the $6P$-, $7S$-, and $5D$-state densities are not uniform.) We estimate, however, that in most cases this trapping is less than a 30% effect on the effective radiative rates except in the cases of $7S\rightarrow 6P$, $5D\rightarrow 6P$, and $7P\rightarrow 7S$. In these cases estimates of trapped radiative rates were made using Holstein's theory.[43,44] In Fig. 4 relative populations n_{nL} divided by the statistical weights g_{nL} are plotted. Multiple entries for the same upper state represent values calculated from different transitions originating from that state. The function e^{-E/kT_e} is also plotted, which represents the populations that would be expected if the levels were in local thermodynamic equilibrium (LTE) at the electron temperature T_e (determined below). Here E is the energy of the relevant level. The data were arbitrarily normalized to e^{-E/kT_e} for the $7D_{5/2}$ state. For levels above $7P$, the observed populations agree fairly well (within approximately a factor of 2) with the value predicted from e^{-E/kT_e}, except for the $4F$ states (which are probably affected fairly strongly by trapping) and the higher P levels (for which transitions from the same upper state to different lower states yield results that are not even self-consistent). However, the transition probabilities of the higher P levels are known to be anomalous and are apparently difficult to calculate. The only other values of these $nP\rightarrow 5D$ transition probabilities that we could find were those of Stone.[45] These values yield results which are in no better agreement with our data than those using Warner's transition probabilities but are discrepant in the opposite sense. Thus we attribute the lack of agreement of predicted and observed P-state densities primarily to inaccuracy in the relevant transition moments. Except for these cases, there is general agreement between the data and the full curve in Fig. 4 which implies that higher states are populated primarily through electron collisions, and are nearly in LTE at the electron temperature. The agreement is not too bad (within a factor of 2 or 3) even for the lower levels given the accuracy of the trapping calculations.

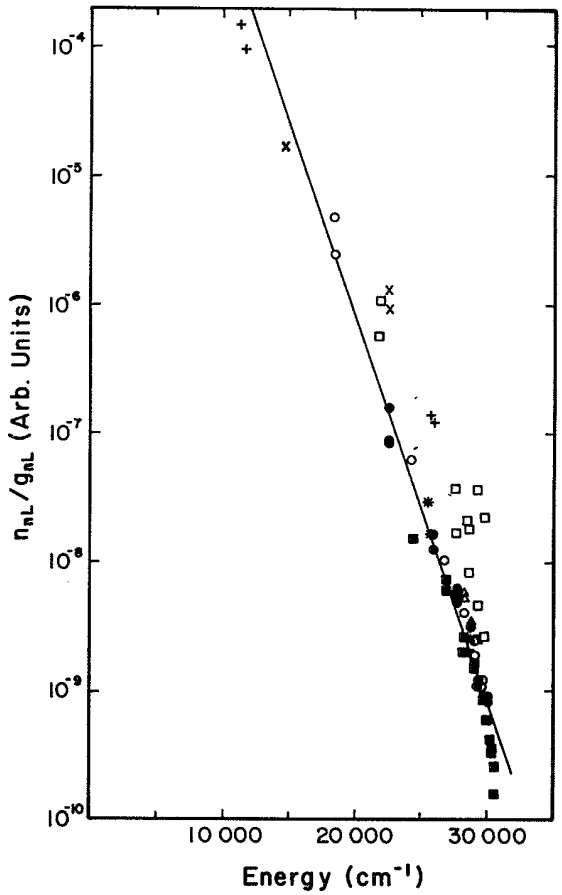

FIG. 4. Plot of n_{nL}/g_{nL}, where n_{nL} is the density of atoms in the nL state and g_{nL} is the statistical weight, vs E_{nL}, the energy of the state above the ground state. Densities were determined from measured line intensities, corrected for detection system efficiency, and the transition probabilities of Refs. 41 and 42. For the $8P\rightarrow 6S$, $7P\rightarrow 6S$, $6P\rightarrow 6S$, and $7S\rightarrow 6P$ transitions, the effective radiative rates were calculated from radiation trapping theory (Refs. 43 and 44). The full curve represents e^{-E/kT_e} with $T_e=2056$ K. The data were arbitrarily normalized to the curve for the $7D_{5/2}$ state ($E=26069$ cm^{-1}). Key: $nP\rightarrow 6S(+)$, $nD\rightarrow 6S(\times)$, $nS\rightarrow 6P(\circ)$, $nD\rightarrow 6P(\bullet)$, $nP\rightarrow 5D(\square)$, $nF\rightarrow 5D(\blacksquare)$, $nP\rightarrow 7S(*)$, $nS\rightarrow 7P(\Delta)$, $nD\rightarrow 7P(\blacktriangle)$.

Figure 5(a) shows the dependences of the $6P_{1/2}\rightarrow 6S_{1/2}$, $5D_{5/2}\rightarrow 6S_{1/2}$, $7P_{1/2}\rightarrow 5D_{3/2}$, $7S_{1/2}\rightarrow 6P_{3/2}$, $10S_{1/2}\rightarrow 6P_{3/2}$, $9D_{3/2}\rightarrow 6P_{1/2}$, and $9F\rightarrow 5D_{5/2}$ fluorescence on laser power. Also shown is the power dependence of the electron density obtained as described below and of the laser power transmitted through the cell at $\lambda=455.7$ nm. As seen in the figure, the transmitted power (and therefore the absorption) was linear in laser power, which indicates that no saturation was occurring, as expected at these Cs densities and laser intensities. Since the laser frequency was subject to drift, and the intensities of spectral lines highly sensitive to laser frequency, care had to be taken in obtaining these power dependences. After the neutral-density filter was inserted and the appropriate line scanned, we repeated the scan with no neutral-density filter present. Data were rejected if the line intensity in the before and after scans (without filter) differed by more than 5%. In the case of the $9F$ fluorescence, intensities were integrated over wavelength using a planimeter to account for the increase in Stark broadening with increasing laser power (see below).

In Fig. 6 we show the spatial distribution of the $6P_{3/2}\rightarrow 6S_{1/2}$, $7P_{1/2}\rightarrow 6S_{1/2}$, $9D_{3/2}\rightarrow 6P_{1/2}$, and $5F_{5/2}\rightarrow 5D_{3/2}$ fluorescence when the laser beam diameter was ~ 2 mm. As can be seen, the red glow extends far beyond the laser-excited column. This is a result of radia-

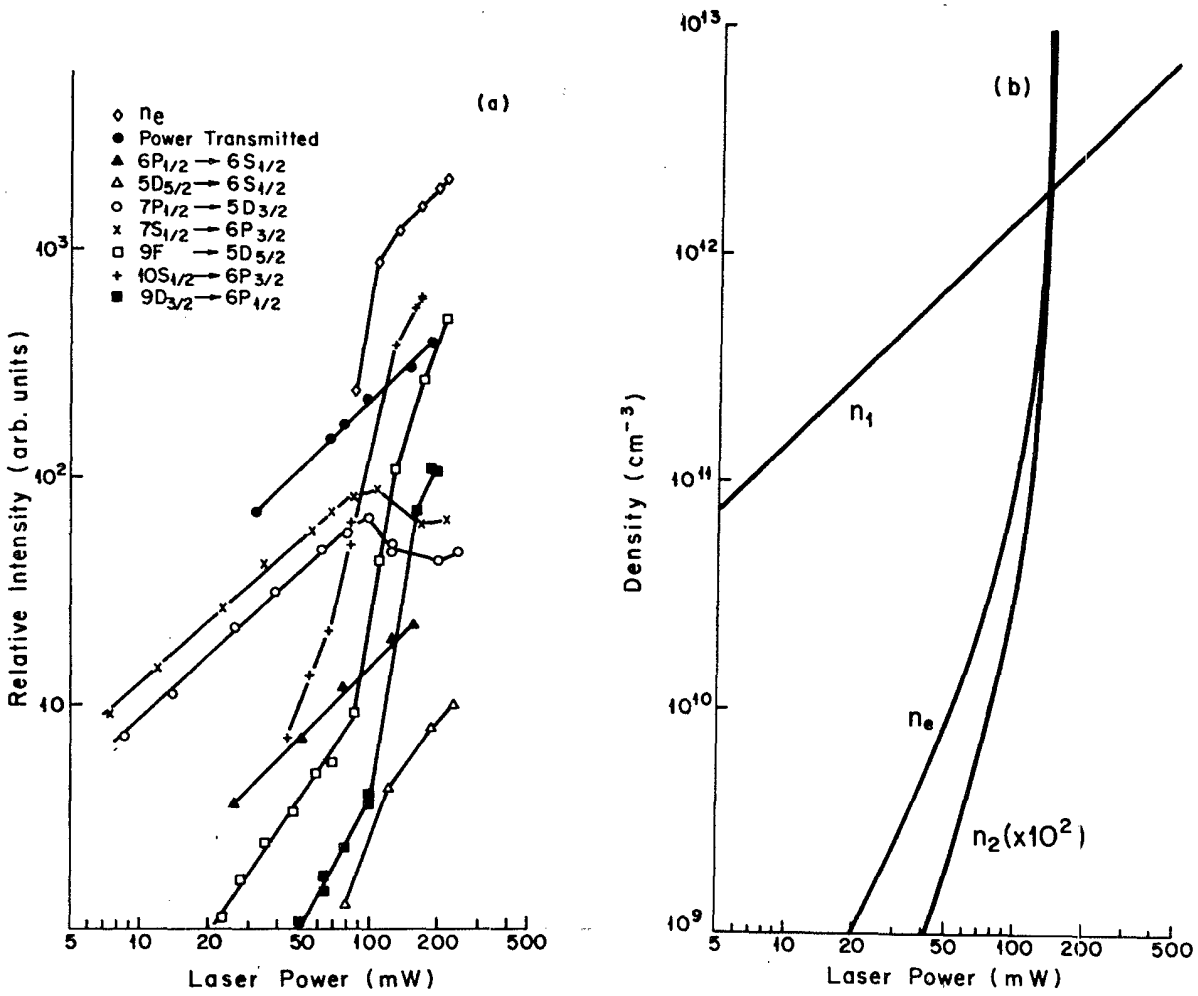

FIG. 5. (a) Atomic fluorescence, electron density, and laser power transmitted through the cell vs laser power, for laser excitation at $\lambda=455.7$ nm ($6S_{1/2}\rightarrow 7P_{3/2}$); $T=250$°C. Each curve is independently normalized. (b) Model calculations of electron, high-lying level and low-lying level densities vs laser power.

tion trapping effects and will be discussed further in Sec. IV.

Figure 7 shows the temperature dependence of the $9D_{3/2}\rightarrow 6P_{1/2}$ fluorescence, which is typical of the other high-lying levels, for excitation at 455.7 nm. We observe a fairly sharp turn on and turn off of this fluorescence at $T\sim 520$ K and $T\sim 600$ K. Evidently this effect appears only for a relatively small range of temperatures. Over the same temperature range, the $7P\rightarrow 6S$ fluorescence shows several minor oscillations (probably due to varying radiation trapping effects on the $7P$, $7S$, $5D$, and $6P$ populations). But over the range 500–625 K, the $7P$ fluorescence is constant to within 25%.

The electron density was estimated from the plasma broadening of the atomic F levels studied using the 0.85 m double monochromator. The broadening of the $9F\rightarrow 5D_{5/2}$ line is easily seen in Fig. 8(a). The inset in the figure shows the unbroadened $9S_{1/2}\rightarrow 6P_{1/2}$ line for comparison. The width of the $9F\rightarrow 5D_{5/2}$ line at $I\sim 220$ mW and $T\sim 250$°C was measured to be 0.47 Å (after subtraction of an instrumental width of ~ 0.22 Å). The Doppler width is $\sim 10^{-2}$ Å. From this we obtain[39] an electron density of 2.05×10^{13} cm^{-3}. In a similar manner the power dependence of the electron density was obtained and is plotted in Fig. 5(a). It is interesting to note that the F levels have asymmetrical line shapes due to the broadening effects of the positive ions (which are slow moving and therefore must be treated in the quasistatic limit) as opposed to the symmetrical broadening arising from the electrons (which are treated in the impact limit)[46] [see Fig. 8(a)].

The electron temperature can be estimated by fitting the blue $Cs_2^+ + e^- \rightarrow Cs(6P) + h\nu$ recombination continuum to the function

$$I(\lambda)\propto \lambda^{-3}\exp\left[\frac{-hc}{kT_e}(\lambda^{-1}-\lambda_{6P}^{-1})\right],$$

where hc/λ_{6P} is the binding energy of the $6P$ state (Ref. 39). In this way we obtain $T_e\sim 2056$ K~ 0.18 eV which is in excellent agreement with the value 0.174 eV predicted from the Saha equation (using the measured n_e) assuming local thermodynamic equilibrium.[47] The observed intensity of the continuum for recombination to $5D$ relative to that for recombination to $6P$ is roughly one to one which is about as expected from our value of T_e and the

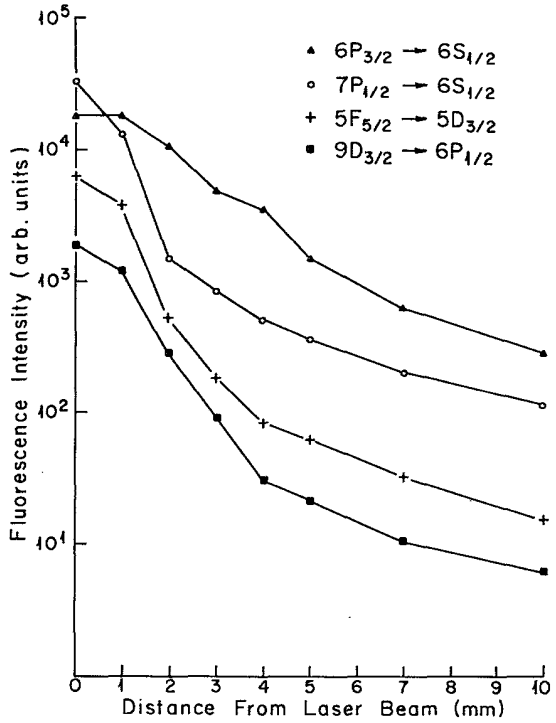

FIG. 6. Spatial distributions of atomic fluorescence for laser excitation at $\lambda=455.7$ nm ($6S_{1/2}\rightarrow 7P_{3/2}$). Laser beam diameter was ~2 mm; $T=250$°C. Each curve is independently normalized.

recombination cross sections of Ref. 39. However, the continuum for recombination to $5D$ is overlapped by a great number of atomic lines which render it less useful for a determination of T_e.

Effects of foreign gas were studied only qualitatively,

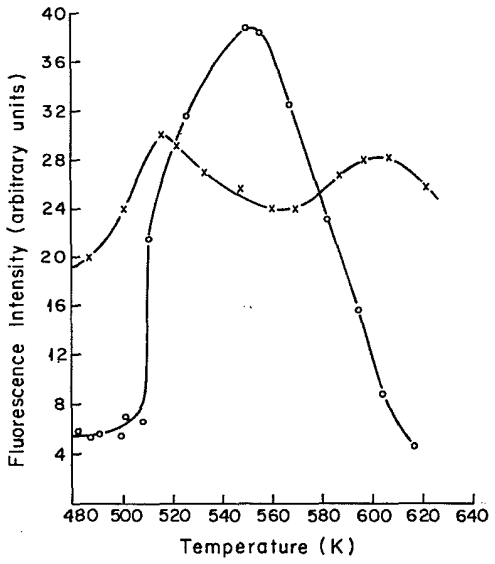

FIG. 7. $9D_{3/2}\rightarrow 6P_{1/2}$(○) and $7P_{1/2}\rightarrow 6S_{1/2}$(×) fluorescence vs temperature for laser excitation at $\lambda=455.7$ nm ($6S_{1/2}\rightarrow 7P_{3/2}$). $9D$ and $7P$ fluorescence are not plotted to the same scale.

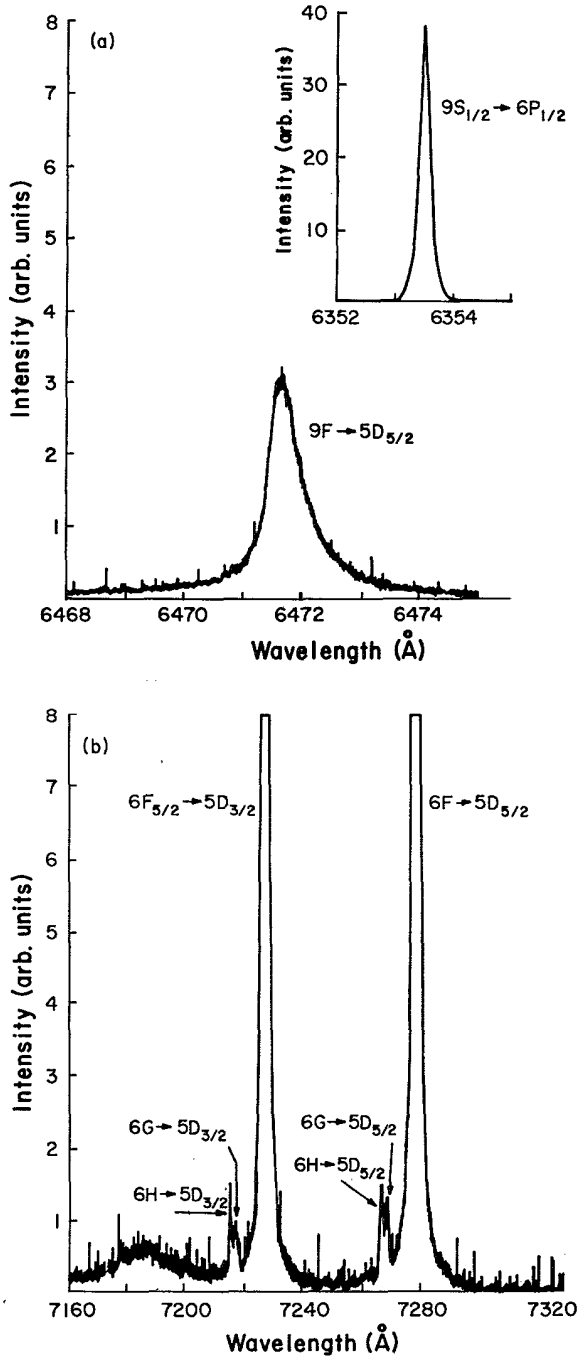

FIG. 8. (a) Electron and ion broadening of the $9F\rightarrow 5D_{5/2}$ line for laser excitation of the Cs $6S_{1/2}\rightarrow 7P_{3/2}$ transition at $\lambda=455.7$ nm; $T=246$°C; $I=220$ mW. Inset shows the unbroadened $9S_{1/2}\rightarrow 6P_{1/2}$ transition. (b) Trace showing the forbidden $6G$, $6H\rightarrow 5D$ lines produced by Stark mixing of the $6F$, $6G$, and $6H$ wave functions. The laser was tuned to the Cs $6S_{1/2}\rightarrow 7P_{3/2}$ transition ($\lambda=455.7$ nm); $T=249$°C; $I=230$ mW. The broad feature between 717 and 720 nm is a diffuse molecular band (see Sec. V and Fig. 10).

but it was found that the presence of argon or neon gas enhanced this "red-glow" effect. This is perhaps due to broadening of the resonance lines which increases the efficiency of the absorption in the line wings.

IV. MODEL AND DISCUSSION OF THE IONIZATION AND POPULATION OF HIGH-LYING LEVELS

A. Cesium

From the power-dependence curves of the high-lying level fluorescence [see $9D_{3/2}\rightarrow 6P_{1/2}$, $9F\rightarrow 5D_{5/2}$, and $10S_{1/2}\rightarrow 6P_{3/2}$ in Fig. 5(a)] and of the electron density, it is evident that at least two separate regimes exist. At low laser powers, the high-lying levels are populated through excited-atom—excited-atom collisions, either directly or by recombination following associative or Penning ionization:

$$\mathrm{Cs}(nL)+\mathrm{Cs}(n'L')\rightarrow \mathrm{Cs}(n''L'')+\mathrm{Cs}(6S)\,, \tag{1}$$

$$\mathrm{Cs}(nL)+\mathrm{Cs}(n'L')\rightarrow \mathrm{Cs}_2^{+}+e^{-}\rightarrow \mathrm{Cs}(n''L'')+\mathrm{Cs}(6S)+h\nu\,, \tag{2}$$

$$\mathrm{Cs}(nL)+\mathrm{Cs}(n'L')\rightarrow \mathrm{Cs}^{+}+e^{-}+\mathrm{Cs}(6S)\rightarrow \mathrm{Cs}(n''L'')+h\nu+\mathrm{Cs}(6S)\,. \tag{3}$$

This excited-atom—excited-atom collisional regime corresponds to the situation in the experiment of Leslie *et al.*[22] in which Cs vapor was excited at the second resonance line by a pulsed laser and fluorescence from high-lying states was also observed. log-log plots of high-lying level fluorescence versus laser power in this regime have slopes that are either near 2 , near 3, or between these two values. A slope of 2 indicates that both states nL and $n'L'$ (possibly the same level) were populated directly by the laser ($7P$) or by cascade from $7P$ (i.e., $7S$, $6P$, and presumably $5D$ all show a linear dependence on laser power in this regime). The large $5D$ population reported in Fig. 4 is significant here since the energies of $6P+5D$ and $5D+5D$ are nearly resonant with several higher levels. In our experiment the $6D\rightarrow 6P$ fluorescence was quadratic in laser power which indicates that $6D$ is populated primarily by $6P$-$6P$ collisions. However, in the pulsed experiment of Leslie *et al.*,[22] the $6D$ fluorescence was linear in laser power indicating that $6D$ was populated there mainly by $7P+6S\rightarrow 6D+6S$ excitation-transfer collisions. Presumably the different $6P$ densities and time scales in the two experiments are responsible for this difference.

A slope near 3 (such as $7D$ or $8D$) on the log-log power-dependence plot indicates that one of the collision partners was itself produced by an excited-atom—excited-atom collision. Intermediate slopes may indicate that more than one population mechanism is operating.

In this power regime the electron density cannot be monitored because it is too low to cause measurable broadening of the F lines. However, presumably it also grows quadratically with power as a result of associative or Penning ionization.

At a laser power of $\sim$100 mW, a threshold is observed in the high-lying level fluorescence versus power curves. Above threshold, the log-log plots of high-lying level fluorescence versus power all display slopes in the range 4—6. Such threshold behavior is suggestive of the "runaway" ionization mechanism

$$\mathrm{Cs}(nL)+e^{-}(mv^2/2)\rightarrow \mathrm{Cs}(6S)+e^{-}(m(v')^2/2=mv^2/2+E_{nL})\,, \tag{4}$$

$$\mathrm{Cs}(n'L')+e^{-}(m(v')^2/2)\rightarrow \mathrm{Cs}^{+}+2e^{-} \tag{5}$$

proposed by Measures[3] to explain the Lucatorto and McIlrath[2] experiment in sodium.

In this mechanism a "cold" electron is heated in a superelastic collision with an excited atom which is thereby quenched to a lower state [Eq. (4)]. After one or more such superelastic collisions, the electron has sufficient kinetic energy to ionize an excited atom [Eq. (5)]. After this ionization, two electrons remain which can undergo the same sequence. Such a mechanism can obviously lead to an exponential growth of the electron density. Atoms in high-lying states can then be produced by recombination or by electron-impact excitation from lower states.

This explanation of the threshold region in the high-lying level populations is strongly supported by our observation of a similar threshold in the electron density occurring at about the same laser power. As the laser power drops from 111 to 87 mW, the electron density drops at least a factor of 3.7. In fact the broadening of the $9F$ level at 87-mW laser power is so low that it is difficult to distinguish it from zero with our resolution. Thus the drop in the electron density in this range may even be greater than Fig. 5(a) indicates.

Detailed models[3,48] based on this mechanism have been developed to explain the runaway ionization in pulsed experiments such as Lucatorto and McIlrath's. These models indicate that a laser pulse duration of a few hundred nanoseconds is necessary to produce such a runaway ionization. This conclusion has been qualitatively verified experimentally (see Ref. 49). For example, with flashlamp laser pumping (pulse duration $\sim$1 μs), almost complete ionization is produced, but with N_2-laser pumped dye-laser excitation (pulse duration $\sim$5 ns) with equivalent or even higher power, only minor ionization occurs. This may point out the most significant difference between the present experiment and that of Leslie *et al.*[22] in which an $\sim$100 ns pulse was used and no threshold effects observed.

To increase the plausibility of the preceding explanation of our results, we have developed a simplified model which demonstrates threshold behavior in the electron and high-lying level populations, using reasonable values for various rate coefficients. Figure 9 shows the simplified energy-level diagram used in the model. The ground-state density n_0 is taken to be constant, since even at the highest laser powers, the densities of all excited and ion levels sum to only a few percent of n_0. Level 1 in the model represents all levels directly pumped by the laser ($7P$) or by cascade from $7P$ ($6P$,$5D$,$7S$). In this model we assume $n_1=n_0P/\Gamma_1=AI$ where n_0P is the laser pumping rate (photons absorbed per cm^3 per second), Γ_1 is the effective radiative rate of level 1 calculated from Holstein's theory of radiation trapping,[43,44] I is the laser power (mW), and A is a constant obtained from absorption measurements. This approximation obviously ignores depletion of n_1 by various collisional processes. Clearly in Fig. 5(a) it can be seen that only the $6P$ population is

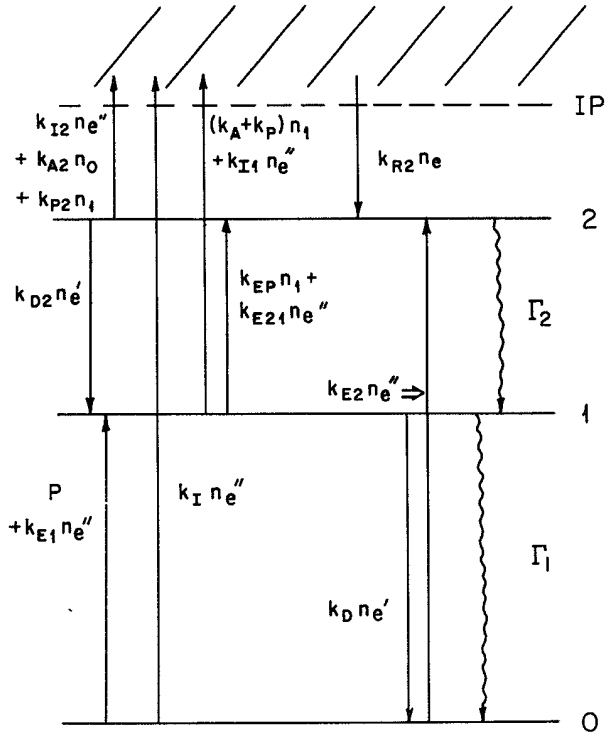

FIG. 9. 3 level energy-level diagram used in the simplified model of the ionization process and subsequent population of high-lying levels. Here level 0 is the ground state, level 1 represents all levels populated directly by the laser or by radiative decay from the pumped level, and level 2 represents all high-lying levels. *IP* is the ionization potential. Most of the collisional and radiative rates used in the model are also shown. *P* is the laser pumping rate and $n_1 \sim (n_0 P/\Gamma_1) \equiv AI$.

truly linear in power. $7S$ and $7P$ are linear below 100 mW but drop at higher powers, while $5D$ rises more rapidly than linearly in that region. These last two effects are due to the complicated interplay of the various electron impact excitation and deexcitation mechanisms (whose net result is that $5D$ is filled at the expense of $7S$ and $7P$). However, these two effects tend roughly to cancel so that the sum of the populations of $6P$, $5D$, $7S$, and $7P$ which equals n_1, is nearly linear with power, and therefore this approximation is reasonable. Level 2 represents all high-lying levels.

We only consider electrons as being either "hot" [those that have undergone a superelastic collision described by Eq. (4)], represented by n_e'', or "cold," represented by n_e'. The total electron density n_e is given by $n_e = n_e'' + n_e'$.

The steady-state rate equation for n_e'' is

$$\dot{n}_e'' = 0 = k_D n_1 n_e' - (k_E + k_I) n_0 n_e'' - D n_e'' - k_R n_e'' n_{Cs^+} , \quad (6)$$

where k_E, k_D, k_I, and k_R are the rate coefficients for electron-impact excitation, deexcitation, and ionization, and for radiative recombination, respectively ($k_E \equiv k_{E1} + k_{E2}$ and $k_R \equiv k_{R0} + k_{R1} + k_{R2}$ in the notation of Fig. 9), and D is the rate of electron diffusion out of the ionization volume. Here we have neglected dissociative recombination which is negligible compared to diffusion at low n_e and negligible compared to radiative recombination at high n_e where $n_{Cs^+} \gg n_{Cs_2^+}$.[39] We have neglected photoionization which should be negligible at our laser powers.[12] Also we have assumed $n_0 \gg n_1 \gg n_2$. The rate equation for cold electrons is

$$\dot{n}_e' = 0 = (k_A + k_P) n_1^2 + (k_E + 2k_I) n_e'' n_0 - k_D n_1 n_e' - D n_e' - k_R n_e' n_{Cs^+} , \quad (7)$$

where k_A and k_P are the rate coefficients for associative and Penning ionization and where the same assumptions have been made as in the hot electron case.

From (6) we obtain

$$n_e'' = \frac{k_D n_1 n_e'}{D + (k_E + k_I) n_0 + k_R n_{Cs^+}} \approx \frac{k_D n_1 n_e'}{(k_E + k_I) n_0} , \quad (8)$$

where in the last step we have neglected D and $k_R n_{Cs^+}$ compared to $(k_E + k_I) n_0$. This is reasonable since $k_E \sim k_I \sim 10^{-7}$ cm^{3}s^{-1},[50,51] $n_0 \sim 10^{16}$ cm^{-3}, $D \sim 10^5$ s^{-1}, (Ref. 52) $k_R \sim 10^{-12}$ cm^{3}s^{-1}, (Ref. 53) and $n_{Cs^+} < 3 \times 10^{13}$ cm^{-3} for our conditions. Adding Eqs. (6) and (7) yields

$$0 = (k_A + k_P) n_1^2 + k_I n_e'' n_0 - D n_e - k_R n_e n_{Cs^+} \approx (k_A + k_P) n_1^2 + \left[\frac{k_I k_D n_1}{k_E + k_I} - D \right] n_e - k_R n_e^2 , \quad (9)$$

where $n_e = n_e' + n_e'' \sim n_e'$ since

$$n_e''/n_e' \sim k_D n_1/(k_E + k_I) n_0 \sim n_1/n_0 < 10^{-3}$$

from Eq. (8), and where $n_{Cs^+} = n_e$ since space charge effects will guarantee that electrons diffuse at roughly the same rate as ions.[52] Equation (9) can be solved for n_e as a function of laser power by using $n_1 = AI$:

$$n_e = \frac{k_I k_D AI}{2k_R(k_E + k_I)} - \frac{D}{2k_R} + \left[\left[\frac{D}{2k_R} - \frac{k_I k_D AI}{2k_R(k_E + k_I)} \right]^2 + \frac{(k_A + k_P) A^2 I^2}{k_R} \right]^{1/2} . \quad (10)$$

Equation (10) is plotted in Fig. 5(b) for reasonable values of the various rate coefficients [$k_I \sim k_E \sim 10^{-7}$ cm^{3}s^{-1} (Refs. 50 and 51), $k_A \sim 10^{-11}$ cm^{3}s^{-1} (Ref. 8 and references therein), $k_R \sim 10^{-12}$ cm^{3}s^{-1} (Ref. 53), $k_P \sim 10^{-9}$ cm^{3}s^{-1} (Refs. 9–11), and $D \sim 10^5$ s^{-1} (Ref. 52)] and the value $A = 1.5 \times 10^{10}$ cm^{-3}/mW estimated from the experiment. As can be seen in the figure, Eq. (10) predicts an approximately quadratic dependence of n_e on I at low power. As power increases a threshold is reached where processes (4) and (5) cause the exponential rise of n_e. Finally at very high power recombination becomes the dominant loss mechanism and n_e approaches a linear dependence on I, assuming the vapor does not first completely ionize.

The rate equation for level 2 is

$$\dot{n}_2 = 0 = k_{EP} n_1^2 + k_{E2} n_0 n_e'' + k_{R2} n_e n_{Cs^+} - k_{A2} n_0 n_2 - k_{P2} n_1 n_2 - k_{D2} n_2 n_e' - k_{I2} n_2 n_e'' - \Gamma_2 n_2 . \quad (11)$$

Here k_{EP} is the Cs(1)+Cs(1)→Cs(2)+Cs(0) "energy-pooling" rate coefficient, k_{A2}, k_{P2}, k_{I2}, and k_{D2} are the rate coefficients for associative ionization, Penning ionization, electron-impact ionization, and electron-impact deexcitation of level-2 atoms, respectively, k_{R2} and k_{E2} are the rate coefficients for radiative recombination and electron-impact excitation to level 2, respectively, and Γ_2 is the level-2 radiative decay rate. In this expression the same approximations were used as in the electron equations. Solving (11) we obtain

$$n_2=\frac{k_{EP}A^2I^2+[k_{E2}k_DAIn_e/(k_E+k_I)]+k_{R2}n_e^2}{k_{A2}n_0+k_{P2}AI+k_{D2}n_e+\Gamma_2}. \quad (12)$$

Using reasonable values of the rate coefficients $k_{D2}\sim k_{E2}\sim k_E\sim k_D\sim k_I\sim 10^{-7}$ cm^{3}s^{-1}, $k_{R2}\sim 10^{-12}$ cm^{3}s^{-1}, $k_{A2}\sim k_A\sim 10^{-11}$ cm^{3}s^{-1}, $k_{EP}\sim 10^{-10}$ cm^{3}s^{-1} (Refs. 54 and 55), $k_{P2}\sim 10^{-9}$ cm^{3}s^{-1}, and $\Gamma_2\sim 2\times 10^7$ s^{-1}, we have calculated n_2 from Eq. (12) and plotted it versus I in Fig. 5(b) along with n_1 and n_e. This simple model qualitatively reproduces the observed power dependences using reasonable values of various rate coefficients and lends credibility to the proposed explanation of the observed ionization and the population of high-lying levels. The saturation of the electron density in the experiment is not, however, reproduced in the model. One reason for this is that our model assumes n_0 is constant. This is not the case when the ionization begins to run away. n_e should obviously also be limited by $n_e<n_0$ ($t=0$). Finally, for high electron densities, our assumption that n_1 is linear in laser power is no longer strictly valid. Clearly, accurate quantitative calculations would require use of a more detailed model (i.e., Refs. 3 or 48) which considers individual energy levels and would also require accurate values of the various rate coefficients. The simple model we present is extremely crude and is not meant for quantitative calculations. It is presented only demonstrate that the ionization we observe is consistent with the mechanism described by Eqs. (4) and (5).

The importance of radiation trapping to the observed ionization phenomenon should be noted. Owing to radiation trapping, the $6P$ population is 2 to 3 orders of magnitude larger than it would be if $6P\rightarrow 6S$ fluorescence photons could escape freely. The large $6P$ population results in trapping of fluorescence from the $7S$ and $5D$ states, thereby causing relatively large populations in these levels and ultimately in the $7P$ level as well. In creating Fig. 4 we have used estimated values of trapped radiative rates for these transitions. These values are, however, very crude due to their dependence on the nonideal geometry and, in the cases where the lower level of the transition is not the ground state, on that excited-state spatial distribution.

The importance of radiation trapping is also evident in the spatial extent of the high-level fluorescence. Figure 6 shows that this fluorescence extends at least 1 cm (in a 1.3-cm-radius cylindrical cell) from the laser axis although the laser beam radius is only ~1 mm. In fact, although the high-level fluorescence was very strongly dependent on laser power, we found that it does not depend strongly on laser intensity. Focusing the laser to increase the intensity (mW/cm^2) by approximately a factor of 100 increased the electron density by less than a factor of 2. The high-lying level fluorescence did not increase significantly in the focused case either. Spatial distributions changed somewhat through the rather minor effect of pump geometry on the radiation-trapping problem. Saturation effects could, however, begin to be seen in the focused case. Clearly, the threshold behavior depends primarily on the total number of photons available rather than on the laser intensity, since, under these conditions, the spatial distribution of the excited atoms (n_1) is determined by trapping of $6P\rightarrow 6S$ photons. Therefore the expression we are using, $n_1=n_0P/\Gamma_1=AI$, contains the laser power I and not the intensity.

The temperature dependence of the high-level fluorescence shown in Fig. 7 is striking, but not yet well understood. A contribution to the high-temperature cutoff results from inability of the laser to penetrate into the vapor, causing the excited atoms to be concentrated near the front window where wall quenching can be important. However, collisional depopulation mechanisms such as excitation transfer to molecules[13] probably are most important in determining the high-temperature cutoff. In fact, molecular emission bands not observed at $T\sim 250$°C do begin to appear as the temperature is raised (see Sec. V). The low-temperature cutoff may be due to low optical depths in the laser wings allowing laser photons to pass through the red-glow region without being absorbed. However, the $7P\rightarrow 6S$ fluorescence remains fairly constant (within ~25%) over a temperature region spanning both cutoffs, indicating that temperature or density effects on electron diffusion may also be significant.

It is interesting to note the very different power dependences of the $7S\rightarrow 6P$ and $5D\rightarrow 6S$ fluorescence intensities [see Fig. 5(a)]. Both upper levels are populated primarily by cascade from the $7P$ level at low powers. However, above threshold, the $5D\rightarrow 6S$ fluorescence increases more rapidly than linearly, while $7S\rightarrow 6P$ actually decreases. In moving toward local thermodynamic equilibrium, $7S$ and $7P$ undergo quenching by electron collisions, while $5D$ receives a net increase in population through such collisions.

B. Rubidium

We have also carried out similar experiments on rubidium vapor, pumping both the first and second resonance levels. In both cases, fluorescence from many high-lying levels and recombination continua were observed. Power dependences were similar to Fig. 5(a) and temperature dependences to Fig. 7. Obviously it is not surprising to obtain similar results in Cs and Rb, but these results demonstrate that direct population of only the first resonance level is sufficient to produce the observed effects.

V. DIFFUSE BANDS

At higher temperatures (around 360°C) the blue laser tuned to the cesium $6S$-$7P$ resonance does not penetrate far into the vapor. The fluorescence is concentrated near the front window and looks blue-white to the eye. Under

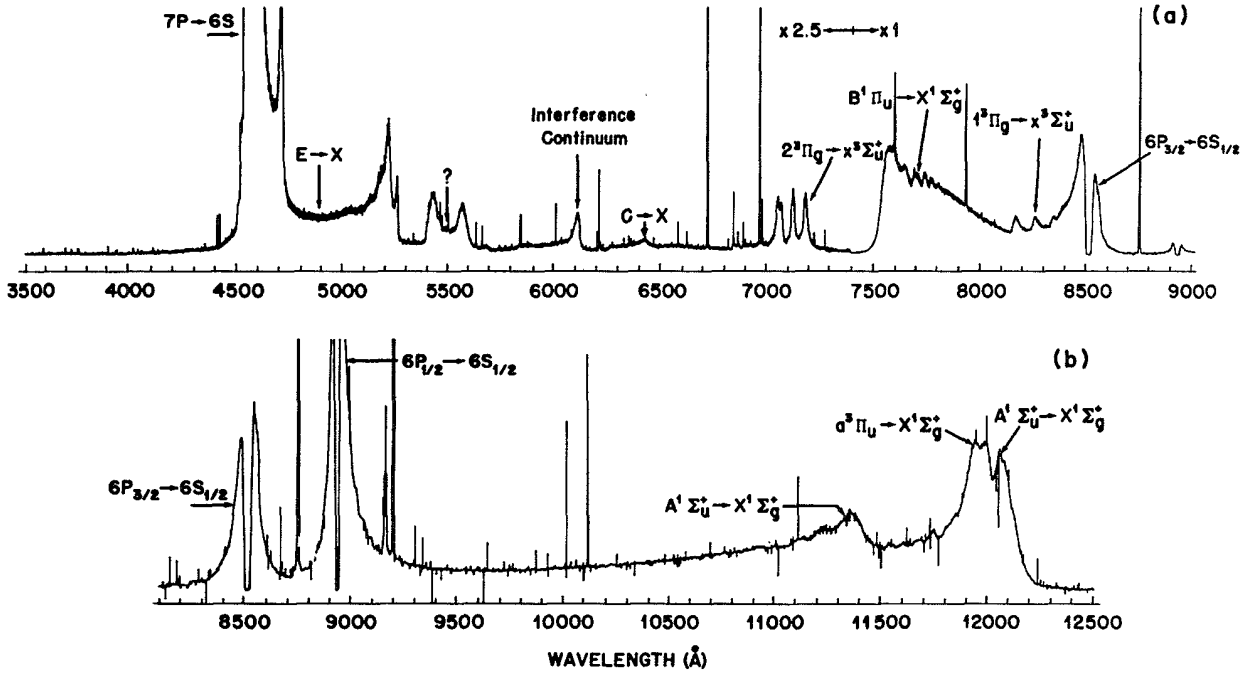

FIG. 10. Cesium molecular fluorescence observed at $T=360$ °C. The laser was detuned slightly from the $6S_{1/2} \rightarrow 7P_{3/2}$ resonance. (a) Visible spectrum observed with the photomultiplier and (b) infrared spectrum observed with the intrinsic germanium detector. In part (b) most of the narrow spikes are due to cosmic rays to which the Ge detector is sensitive.

these conditions very little atomic emission remains and the spectrum is dominated by diffuse-looking molecular bands. Such a spectrum is shown in Fig. 10 where the laser was detuned a few GHz from the $6S \rightarrow 7P_{3/2}$ resonance to further suppress the atomic emission which is very sensitive to detuning. The molecular emissions are not as sensitive to detuning although they do decrease with increasing detuning from the $6S \rightarrow 7P$ resonance.

The spectrum contains a broad band with satellite features near 472, 523, and 527 nm which can be identified with the Cs_2 "E" absorption band.[27,30,32] This band is now thought to consist of more than one electronic transition whose lower state is the $X\,^1\Sigma_g^+$ ground state of the molecule and whose upper states dissociate to $7P+6S$.[56,57] Presumably in the present experiment these states are populated in excitation-transfer collisions between $7P$ atoms and ground-state molecules: $Cs(7P)+Cs_2(X\,^1\Sigma_g^+) \rightarrow Cs(6S)+Cs_2(E)$.

The weak feature between 625 and 680 nm is emission on the well-known $C\,^1\Pi_u \rightarrow X\,^1\Sigma_g^+$ transition.[27,29,58,59] Presumably the upper state is populated through excitation-transfer collisions of ground-state molecules with $7S$ or $5D$ atoms.

The strong band extending to the blue of the $6S_{1/2} \rightarrow 6P_{3/2}$ atomic resonance line (852.1 nm) with a maximum at ~760 nm, is the well-known Cs_2 $B\,^1\Pi_u \rightarrow X\,^1\Sigma_g^+$ band which also has been studied extensively.[27,29,30,32] The oscillatory structure between 763 and 783 nm which can be seen in Fig. 10 reproduces similar structure observed in absorption.[32]

The band peaking at ~610 nm can be identified as the longest wavelength and most intense peak of the diffuse bands previously observed between ~570 and 610 nm.[34–38,40,60] It is now generally believed that this fluorescence represents emission from bound states of an upper potential well to continuum states of the ground $X\,^1\Sigma_g^+$ state. The upper well is most likely displaced to larger internuclear separation than the lower state which permits classical Franck-Condon principle allowed transitions to the lower continuum levels. Tellinghuisen *et al.*[38] make convincing arguments that the upper state of these transitions is not the same as that responsible for the bound-bound emission at $\lambda < 527$ nm. Instead they argue that the upper state of the 610-nm bands is located at large internuclear separation due to a strong ion-pair character. Pichler *et al.*[60] suggest the upper state of the analogous Rb band is actually a double-minimum state.

The four narrow bands observed here between 700 and 720 nm (the 705 and 707 nm bands are just resolved in Fig. 10) were first observed in absorption by Walter and Barratt[61] in 1928. Loomis and Kusch[27] studied these bands (also in absorption) in 1934 using a high-resolution spectrograph and reported that the 707 nm peak actually contains three sharp edges. (These edges may also be seen in the absorption spectra of Ref. 62.) These bands are now believed to correspond to transitions to the mainly repulsive $x\,^3\Sigma_u^+$ state which dissociates to two ground-state atoms.[32] They are thought to be analogous to the sodium violet bands[63–69] (λ=416–457 nm), the potassium yellow bands[61,68–72] (λ=560–580 nm), and the Rb_2 590–620-nm bands.[61,40,73,60] Recently Li and Field[74] directly identified the upper state of the Na_2 violet bands as the second lowest $^3\Pi_g$ using optical-optical double resonance fluorescence excitation spectroscopy. The fluorescence bands therefore represent $2\,^3\Pi_g \rightarrow x\,^3\Sigma_u^+$ transitions. In the heavy Cs_2 molecule the Hund's case (a) notation is not strictly applicable. The $^3\Pi_g$ state would correspond to 2_g, 1_g, 0_g^+, and 0_g^- in Hund's case (c) while the $^3\Sigma_u^+$ corre-

sponds to 1_u and 0_u^-. Six allowed transitions exist between these levels which agrees with the observed fluorescence spectrum (assuming the 707-nm band actually consists of three different electronic transitions). Pichler *et al.*[62] have shown that the splittings between these bands is explained by the strong ionic character $[Cs^+(^1S)+Cs^-(^3P)]$ of the $2\,^3\Pi_g$ states. Additionally they suggest that the shapes of these potentials are influenced by interaction with the $1^3\Pi_g$ states.

The four diffuse peaks we observe at 817, 827, 835, and 840 nm were first observed by Loomis and Kusch[27] who found them to be truly diffuse under high resolution. Kusch and Hessel[29] attributed these bands to weak predissociation of high vibrational levels of the $B^1\Pi_u$ state by repulsive triplet states. We believe these bands, which we observe here in emission, represent transitions analogous to the $1^3\Pi_g \rightarrow x^3\Sigma_u^+$ satellite bands which have been observed in the blue wings of the first resonance lines of the lighter alkalis.[75–77] Just as the large spin-orbit coupling in Cs causes the 700–720-nm $2^3\Pi_g \rightarrow x^3\Sigma_u^+$ band to split into separate fine-structure components, so too we expect the same to happen with this $1^3\Pi_g \rightarrow x^3\Sigma_u^+$ transition. Since both lower and upper states are repulsive, the bands are truly diffuse. We note that the identification we make here between the observed diffuse bands at 817, 827, 835, and 840 nm and the $1^3\Pi_g \rightarrow x^3\Sigma_u^+$ satellite bands is based only on analogy and not on quantitative evidence. Further experiments will be needed to confirm this identification.

Beneath the forbidden $5D \rightarrow 6S$ transitions we see weak molecular emissions which have previously been studied by Niemax.[78]

In the near infrared we observe strong $A^1\Sigma_u^+ \rightarrow X^1\Sigma_g^+$ band emission with maxima near 1.14 and 1.21 μm. This band has been studied extensively in the past.[27,28,31,33] The gap between the two maxima has been attributed by Benedict *et al.*[31,33] to perturbations of the energy levels at the crossing of the $A^1\Sigma_u^+$ state and the more deeply bound $a^3\Pi_u$ state. The maxima at 1.20 μm is attributed by them to be $a^3\Pi_u \rightarrow X^1\Sigma_g^+$ transitions which are allowed in the heavy Cs_2 molecule, while the 1.21 μm peak is attributed to $A^1\Sigma_u^+ \rightarrow X^1\Sigma_g^+$ transitions.

The most interesting feature in Fig. 10 is the double humped emission appearing between 540 and 560 nm. To the best of our knowledge it has only been mentioned briefly once before in the literature. This reference was by Tam *et al.*[79] who observed this feature in pure Cs vapor and cesium-helium mixtures with laser excitation at 457.9 nm. This band could conceivably have its origins in impurities, but we believe this explanation can be eliminated since the temperature dependence of the emission intensity is the same as that for the known Cs_2 bands. The most likely sources of this emission, based on energetics, are either fluorescence to the $x^3\Sigma_u^+$ state from bound states of the $7P+6S$ or $6P+6P$ manifold or fluorescence to the $X^1\Sigma_g^+$ state from bound states of the $7S+6S$ manifold. The last possibility is eliminated by the absence of this band in absorption, while the fact that the emission has only been observed when large excited atom populations exist, may favor the explanation based on emission from the $6P+6P$ manifold.

We note that all of these molecular emission features scale roughly linearly with laser power, indicating that none of them originate from above the $7P+6S$ manifold.

At first glance the observation of molecular emission under these conditions of rapid collisional mixing and high optical depths may seem hopelessly confusing. However, this situation has certain advantages such as the selective self-attenuation of the well-known transitions involving the ground $X^1\Sigma_g^+$ state. According to the data of Refs. 30 and 32, the E and C band emissions are attenuated by $\sim 30\%$ in traversing the cell to our detector while the B and A bands may be attenuated by a factor of 10 or more. Additionally, the very strong radiation trapping of the $6P \rightarrow 6S$ resonance radiation reduces those line center emission peaks by 10^2–10^3 and forces the radiation out into the line wings where far wing spectra and satellite features can then be observed. In this sense we effectively have not only highly selective D_1 and D_2 line filters in the experiment, but they are filters which force unwanted light into spectral regions of interest rather than simply absorbing it. The heavy trapping of resonance radiation and the large population in the $6P$ state due to pumping of an atomic transition (which feeds $6P$ through cascade), may also result in many excited atom-excited atom collisions. Thus bands whose upper state belongs to the $6P+6P$ manifold might be studied using this technique although nothing we observe here may obviously be so identified.

We also observed similar band structure in rubidium vapor excited at the $5S \rightarrow 6P$ atomic transition. This included the diffuse bands between 590 and 620 nm, the $B\,^1\Pi_u$–$X\,^1\Sigma_g^+$ band[80] between 640 nm and the first resonance lines, and another feature between ~ 420 and 510 nm which probably can be identified with the known Rb_2 C and D absorption bands.

VI. CONCLUSIONS

We report here the observation of ionization and the population of high-lying atomic levels in cesium vapor excited at the second resonance transition $6S$-$7P$. Through a simple model we have shown that the ionization increases rapidly with laser power due to fast electron impact ionization where the electrons were previously heated in superelastic collisions with excited atoms. The populations of the high-lying levels were shown to be close to local thermodynamic equilibrium. Spatial resolution of the atomic emissions demonstrates the role of radiation trapping in this process. We have also seen that these processes occur only in a limited range of temperatures. Similar studies on rubidium demonstrate that the same types of processes can occur when the first resonance line is excited. At higher temperatures diffuse molecular emission features appear. Some of these features may be identified as transitions to the repulsive $x^3\Sigma_u^+$ state.

Note added. After preparation of this manuscript, we learned that the 810–850-nm diffuse bands in Cs_2 have been investigated experimentally and theoretically by Niemax, Pichler, and co-workers. These detailed studies confirm the identification made here that these bands

represent the Cs_2 analog of the $1^3\Pi_g$-$x^3\Sigma_u^+$ satellites observed in the blue wing of the first resonance doublet of the lighter alkalis [G. Pichler, R. Beuc, D. Veza, S. Milosevic, and K. Niemax (private communications)]. Early results of the Niemax, Pichler *et al.* work on these bands were presented at the 1978 Molecular Spectroscopy Conference in Columbus, Ohio. The complete study will soon be submitted for publication.

ACKNOWLEDGMENTS

We would like to thank Dr. Will Happer, Dr. Alan Gallagher, Dr. Andy Tam, Dr. Nat Bhaskar, and Dr. Goran Pichler for many useful discussions throughout the course of this work. This work was supported under Grants Nos. DAAG-29-81-K-0011 and DAAG-29-83-K-0072 from the U.S. Army Research Office.

*Current address: Lehigh University, Department of Physics, Physics Building 16, Bethlehem, PA 18015.

[1]M. Allegrini, G. Alzetta, K. Kopystynska, L. Moi, and G. Orriols, Opt. Commun. **19**, 96 (1976).
[2]T. B. Lucatorto and T. J. McIlrath, Phys. Rev. Lett. **37**, 428 (1976).
[3]R. M. Measures, J. Appl. Phys. **48**, 2673 (1977).
[4]A. Klyucharev, V. Sepman, and V. Vuinovich, Opt. Spektrosk. **42**, 588 (1977) [Opt. Spectrosc. (USSR) **42**, 336 (1977)].
[5]A. de Jong and F. van der Valk, J. Phys. B **12**, L561 (1979).
[6]V. S. Kushawaha and J. J. Leventhal, Phys. Rev. A **22**, 2468 (1980); **25**, 346 (1982).
[7]R. Bonanno, J. Boulmer, and J. Weiner, Phys. Rev. A **28**, 604 (1983).
[8]J. Huennekens and A. Gallagher, Phys. Rev. A **28**, 1276 (1983).
[9]M. Chéret, A. Spielfiedel, R. Durand, and R. Deloche, J. Phys. B **14**, 3953 (1981).
[10]M. Chéret, W. Lindinger, L. Barbier, and R. Deloche, Chem. Phys. Lett. **88**, 229 (1982).
[11]M. Chéret, L. Barbier, W. Lindinger, and R. Deloche, J. Phys. B **15**, 3463 (1982).
[12]A. V. Smith, J. E. M. Goldsmith, D. E. Nitz, and S. J. Smith, Phys. Rev. A **22**, 577 (1980).
[13]L. K. Lam, T. Fujimoto, and A. C. Gallagher, J. Chem. Phys. **68**, 3553 (1978).
[14]A. Sharma, N. D. Bhaskar, Y. Q. Lu, and W. Happer, Appl. Phys. Lett. **39**, 209 (1981).
[15]B. Wellegehausen, W. Luhs, A. Topouzkhanian, and J. D'Incan, Appl. Phys. Lett. **43**, 912 (1983).
[16]P. Bernage, P. Niay, and H. Bocquet, J. Mol. Spectrosc. **98**, 304 (1983).
[17]W. Müller and I. V. Hertel, Appl. Phys. **24**, 33 (1981).
[18]W. Müller, J. J. McClelland, and I. V. Hertel, Appl. Phys. B **31**, 131 (1983).
[19]C. E. Moore, *Atomic Energy Levels,* Natl. Bur. Stand. (U.S.) Circ. No. 467 (U.S. GPO, Washington, D. C., 1948, 1952, and 1958), Vols. I–III.
[20]A. C. Tam (private communication).
[21]N. D. Bhaskar (private communication).
[22]S. G. Leslie, J. T. Verdeyen, and W. S. Millar, J. Appl. Phys. **48**, 4444 (1977).
[23]A. C. Tam and W. Happer, Opt. Commun. **21**, 403 (1977).
[24]A. C. Tam, J. Appl. Phys. **51**, 4682 (1980).
[25]J. T. Bahns and W. Stwalley (unpublished).
[26]M. E. Koch, K. K. Verma, J. T. Bahns, and W. C. Stwalley, in *Proceedings of the International Conference on Lasers '82, New Orleans, 1982,* edited by Richard C. Powell (STS, McLean, Va., 1982).
[27]F. W. Loomis and P. Kusch, Phys. Rev. **46**, 292 (1934).
[28]D. S. Bayley, E. C. Eberlin, and J. H. Simpson, J. Chem. Phys. **49**, 2863 (1968).
[29]P. Kusch and M. M. Hessel, J. Mol. Spectrosc. **32**, 181 (1969).
[30]G. Moe, A. C. Tam, and W. Happer, Phys. Rev. A **14**, 349 (1976).
[31]R. P. Benedict, D. L. Drummond, and L. A. Schlie, J. Chem Phys. **66**, 4600 (1977).
[32]R. Gupta, W. Happer, J. Wagner, and E. Wennmyr, J. Chem. Phys. **68**, 799 (1978).
[33]R. P. Benedict, D. L. Drummond, and L. A. Schlie, J. Chem. Phys. **70**, 3155 (1979).
[34]R. J. Exton, W. L. Snow, and M. E. Hillard, J. Quant. Spectrosc. Radiat. Transfer **20**, 235 (1978).
[35]G. Honing, M. Czajkowski, M. Stock, and W. Demtroder, J. Chem. Phys. **71**, 2138 (1979).
[36]H. Kato and K. Yoshihara, J. Chem. Phys. **71**, 1585 (1979).
[37]H. Kato, Int. J. Quantum Chem. **18**, 287 (1980).
[38]J. Tellinghuisen, G. Pichler, W. L. Snow, M. E. Hillard, and R. J. Exton, Chem. Phys. **50**, 313 (1980).
[39]L. Agnew and W. H. Reichelt, J. Appl. Phys. **39**, 3149 (1968).
[40]M. McClintock and L. C. Balling, J. Quant. Spectrosc. Radiat. Transfer **9**, 1209 (1969).
[41]B. Warner, Mon. Not. R. Astron. Soc. **139**, 115 (1968).
[42]M. Fabry, J. Quant. Spectrosc. Radiat. Transfer **16**, 127 (1976).
[43]T. Holstein, Phys. Rev. **72**, 1212 (1947).
[44]T. Holstein, Phys. Rev. **83**, 1159 (1951).
[45]P. M. Stone, Phys. Rev. **127**, 1151 (1962).
[46]H. R. Griem, *Plasma Spectroscopy* (McGraw-Hill, New York, 1964).
[47]D. Mihalas, *Stellar Atmospheres* (Freeman, San Francisco, 1978).
[48]G. A. Victor and G. Lafyatis (unpublished).
[49]R. Kunnemeyer and M. Kock, J. Phys. B **16**, L607 (1983).
[50]I. C. Percival, Nucl. Fusion **6**, 182 (1966).
[51]D. H. Crandall, G. H. Dunn, A. Gallagher, D. G. Hummer, C. V. Kunasz, D. Leep, and P. O. Taylor, Astrophys. J. **191**, 789 (1974).
[52]Electrons diffuse at the ambipolar diffusion rate determined roughly by the ion velocity ($\sim 5\times 10^4$ cm/s).
[53]D. W. Norcross and P. M. Stone, J. Quant. Spectrosc. Radiat. Transfer **6**, 277 (1966).
[54]T. Yabuzaki, A. C. Tam, M. Hou, W. Happer, and S. M. Curry, Opt. Commun. **24**, 305 (1978).
[55]J. Huennekens and A. Gallagher, Phys. Rev. A **27**, 771 (1983).
[56]G. Baumgartner, W. Demtroder, and M. Stock, Z. Phys. **232**, 462 (1970).
[57]Z. Wu and J. Huennekens, J. Chem. Phys. **81**, 4433 (1984).
[58]P. Kusch and M. M. Hessel, J. Mol. Spectrosc. **25**, 205 (1968).
[59]M. Raab, G. Honing, W. Demtroder, and C. R. Vidal, J. Chem. Phys. **76**, 4370 (1982).
[60]G. Pichler, S. Milosevic, D. Veza, and D. Vukicevic, J. Phys. B **16**, 4633 (1983).
[61]J. M. Walter and S. Barratt, R. Soc. Proc. A **119**, 257 (1928).
[62]G. Pichler, S. Milosevic, D. Veza, and R. Beuc, J. Phys. B **16**, 4619 (1983).
[63]M. Allegrini, G. Alzetta, A. Kopystynska, L. Moi, and G. Or-

riols, Opt. Commun. **22**, 329 (1977).
[64]J. P. Woerdman, Opt. Commun. **26**, 216 (1978).
[65]A. Kopystynska and P. Kowalczyk, Opt. Commun. **28**, 78 (1979).
[66]M. Allegrini and L. Moi, Opt. Commun. **32**, 91 (1980).
[67]C. Y. R. Wu and J. K. Chen, Opt. Commun. **44**, 100 (1982).
[68]G. Pichler, S. Milosevic, D. Veza, and S. Bosanac, in *Spectral Line Shapes,* edited by K. Burnett (Walter de Gruyter, Berlin, 1983), Vol. II, p. 613.
[69]Cz. Radzewicz, P. Kowalczyk, and J. Krasinski, Opt. Commun. **44**, 139 (1983).
[70]M. M. Rebbeck and J. M. Vaughan, J. Phys. B **4**, 258 (1971).
[71]Yu. P. Korchevoi, V. I. Lukashenko, and S. N. Lukashenko, Zh. Eksp. Teor. Fiz. **75**, 846 (1978) [Sov. Phys.—JETP **48**, 428 (1978)].
[72]Yu. P. Korchevoi, V. I. Lukashenko, and S. N. Lukashenko, Phys. Scr. **19**, 271 (1979).
[73]J. M. Brom and H. P. Broida, J. Chem. Phys. **61**, 982 (1974).
[74]Li Li and R. W. Field, J. Phys. Chem. **87**, 3020 (1983).
[75]D. Veza, J. Rukavina, M. Movre, V. Vujnovic, and G. Pichler, Opt. Commun. **34**, 77 (1980).
[76]D. Veza, S. Milosevic, and G. Pichler, Chem. Phys. Lett. **93**, 401 (1982).
[77]R. Beuc, S. Milosevic, M. Movre, G. Pichler, and D. Veza, Fizika **14**, 345 (1982).
[78]K. Niemax, J. Quan. Spectrosc. Radiat. Transfer **17**, 125 (1977).
[79]A. Tam, G. Moe, W. Park, and W. Happer, Phys. Rev. Lett. **35**, 85 (1975).
[80]C. D. Caldwell, F. Engelke, and H. Hage, Chem. Phys. **54**, 21 (1980).